JOURNAL OF Applied Polymer SCIENCE

Special Issue: Sustainable Polymers and Polymer Science Dedicated to the Life and Work of Richard P. Wool

Guest Editors: Dr Joseph F. Stanzione III (Rowan University, U.S.A.)
and Dr John J. La Scala (U.S. Army Research Laboratory, U.S.A.)

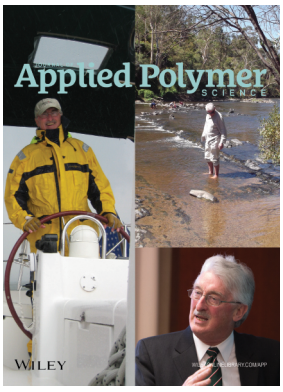

EDITORIAL

REVIEWS

RESEARCH ARTICLES

JOURNAL OF Applied Polymer SCIENCE

Special Issue: Sustainable Polymers and Polymer Science Dedicated to the Life and Work of Richard P. Wool

Guest Editors: Dr Joseph F. Stanzione III (Rowan University, U.S.A.)
and Dr John J. La Scala (U.S. Army Research Laboratory, U.S.A.)

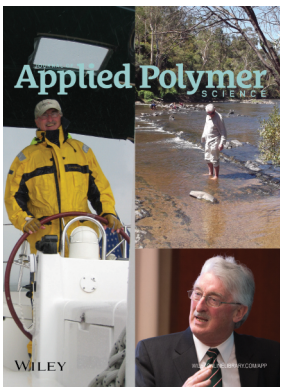

Journal of Applied Polymer Science

Biorenewable blends of polyamide-4,10 and polyamide-6,10

Christopher S. Moran,[1] Agathe Barthelon,[1] Andrew Pearsall,[1] Vikas Mittal,[2] John R. Dorgan[1]
[1]Department of Chemical and Biological Engineering, Colorado School of Mines, Golden, Colorado 80401
[2]Department of Chemical Engineering, Petroleum Institute, Abu Dhabi, United Arab Emirates
Correspondence to: J. R. Dorgan (E-mail: jdorgan@mines.edu)

ABSTRACT: Biobased polymers hold the promise of greatly improved sustainability metrics. In this study, semicrystalline polymer blends are formulated between two partially biorenewable polyamides. Polyamide 4,10 (PA410) is melt mixed with polyamide-6,10 (PA610). Physical properties of the blends are investigated using differential scanning calorimetry (DSC), thermal gravimetric analysis (TGA), dynamic mechanical thermal analysis (DMTA), impact testing, and tensile testing. Morphological features are studied using small angle X-ray scattering (SAXS) and wide angle X-ray scattering (WAXS). *The previously unreported equilibrium enthalpy of fusion for PA410 is found to be 269 J/g.* Melting point depression from DSC is used to establish miscibility and calculate the polymer–polymer interaction parameter which is approximately independent of composition and equal to −0.25 kJ/mol. Crystallization induced phase separation is observed wherein crystallization drives phase separation. SAXS exhibits an increase in lamellar long spacing with increasing PA610 content. WAXS confirms the presence of only PA410 and PA610 crystals. The mechanical properties of the blends are shown to deviate from a simple law of mixtures. This miscible biorenewable polymer blend, exhibiting crystallization induced phase separation, and characterized by superior properties is of both scientific and potential commercial interest. © 2016 Wiley Periodicals, Inc. J. Appl. Polym. Sci. **2016**, *133*, 43626.

KEYWORDS: biopolymers & renewable polymers; blends; mechanical properties; polyamides; X-ray

Received 18 November 2015; accepted 14 March 2016
DOI: 10.1002/app.43626

INTRODUCTION

Global production capacity of biopolymers is expected to grow from 1.6 million metric tons in 2013 to 6.7 million metric tons in 2018.[1] The majority of this growth is attributed to bio-based nondegradable polymers rather than biodegradable polymers. Demand for bio-based polymers is increasing due to several factors—as a strategy to mitigate environmental impacts, because of new technical developments that provide better price-performance characteristics thereby expanding application areas, and due to consumers' increasing desire for more sustainable products.[1–4]

The pioneering commercially successful bioplastic was the polyester PLA (polylactide) which is now produced in many locations across the globe.[5–10] PLA has been quantitatively shown to have superior environmental attributes when compared to other polymeric materials.[11–15] In contrast to biobased polyesters such as PLA, this study evaluates binary blends of Nylon 4,10 (PA410) and Nylon 6,10 (PA610); these two engineering polyamides have recently been made available from renewable resources.

Nylons (or polyamides) have been used for numerous applications since their original development in the 1930s. These polymers were traditionally used as fibers,[16] an application area shared with PLA.[17–21] However, polyamides now have a wide range of application including injection molded and extruded engineering parts. Polyamides are a commercial success story for polymer nanocomposites.[22–27] Today there are many polyamide grades including various glass fiber and other filled materials; they are considered engineering thermoplastic materials. Given the widespread utilization of polyamides and the potential environmental advantages of utilizing renewable resources, there is a tremendous opportunity to develop classes of more sustainable plastics.

Commercial developments have led to the cost-effective production of bio-based sebacic acid, a 10-carbon diacid derived from castor oil that can be polymerized with various diamines to produce polyamides.[28,29] The PA410 and PA610 used in this study are both made from bio-based sebacic acid. Accordingly, each of the homopolymers and blends thereof has a renewable carbon content ranging from 63% to 71%. Their respective 4-carbon and 6-carbon diamine counterparts, butanediamine and

Additional Supporting Information may be found in the online version of this article.

hexanediamine, are typically derived from petroleum. However, butanediamine can be derived from the commercially available bio-based succinic acid, and also from direct fermentation of sugars.[28] Routes to hexanediamine are also possible via adipic acid or direct fermentation.[28,30,31] Future developments leading to commercial availability of 100% renewable PA410 and PA610 are presumable. Accordingly, investigation of their blends as a means of achieving varying properties is of great interest now and into the future.

Polymer blending is a well-established and cost-effective technique to engineer new materials with tunable physical properties.[32–36] Miscible polymer blends are rare because the long range order of polymer chains limits the entropy of mixing to small values. Even though the enthalpy of mixing is also usually a small value, it can be enough to cause a positive free energy of mixing, meaning that mixing is not thermodynamically spontaneous. Therefore, most polymers stay phase separated when physically mixed together. For very small enthalpies of mixing, or for negative values, the polymer mixture is miscible. The morphology of immiscible blends often leads to undesirable physical properties, so much of the effort in polymer blending research is focused on physical and chemical compatibilization techniques to alter morphology.[32,34,35,37–43] Clearly, if additional reagents and processes are not needed, blending becomes more cost-effective; accordingly, miscible polymer blends are of great interest.

The goal of this study is to investigate the morphology and physical property relationships of PA410 blended with PA610. There have been numerous reports on blends of bio-degradable polymers, particularly for medical or packaging applications.[32,44–52] However, relatively limited research is reported on bio-based polymer blends for high-performance material applications.[32–34,53,54] Polyamide blend literature is typically concerned with aliphatic polyamides blended with aromatic polyamides.[55–62] Few studies have been reported on purely aliphatic blends.[60,63–66]

An essential part to understanding the PA410 and PA610 binary system is to determine its miscibility. There are many experimental techniques to determine if polymers are miscible. [37,55,56,67–76] Two of the most convincing pieces of experimental evidence that suggest blends are miscible are melting point depression and the presence of only one glass transition temperature. Miscible aliphatic polyamides are rare but possible. Of all the reported miscible polyamide blends, including polyamide 4,8/polyamide 6,6,[64] polyamide 6,6/polyamide 6,[60,66] and polyamide 11/polyamide 6,10,[63] it is important to note that the *average number of backbone carbon atoms between repeating amide groups in each homopolymer is similar.* This general trend is consistent with the findings of the current investigation.

EXPERIMENTAL

Materials

Ultramid Balance PA610 was provided by Dr. Scherzer from BASF SE (Ludwigshafen, Germany). EcoPaXX Q150MS PA410 from DSM (Netherlands) was obtained from Chase Plastics. The thermal stabilizers, Irganox 1076 and Irgafos 168, were donated by BASF Chemical Company and stored under argon. Reagent grade anhydrous toluene was purchased from Sigma-Aldrich.

Methods

PA410 was melt blended with PA610 at wt % PA410/PA610 compositions of 0/100, 20/80, 40/60, 50/50, 60/40, 80/20, and 100/0 in a Haake Rheomix 300 with roller blades. The polymers were dried under vacuum (23 in. Hg) at 80 °C for 3 days prior to mixing to reduce hydrolysis. After complete melting was achieved at 260 °C, thermal stabilizers were added as solutions in toluene so that on evaporation of toluene, the blends would contain 0.25 wt % of each stabilizer relative to PA610. After the addition of stabilizer, the blends were mixed at 50 RPM for 10 min, then removed from the mixing bowl using a spatula and allowed to cool to room temperature. Subsequently, the cooled material was ground to a pellet size of 2–3 mm in a Foremost A2 granulator. The recovered pellets were dried under vacuum for 3 days at 80 °C and then injected molded into rectangular or dog bone shaped bars using a benchtop injection molding machine (Morgan Press). To ensure reproducibility of results, sample bars were annealed to achieve the maximum degree of crystallinity and aged to ensure relaxation of free volume; this was accomplished by crystallizing at 180 °C for 3 days and aging at room temperature for at least 1 week prior to any type of mechanical testing. To investigate the effect of crystallinity on the physical properties and morphology, additional sample bars were aged for at least 1 week without annealing.

Solution blended samples were prepared for determination of melting point depression in DSC studies. Solutions with wt % PA410/PA610 compositions of 0/100, 20/80, 40/60, 50/50, 60/40, 80/20, and 100/0 were dissolved completely in m-cresol at 0.1 g/mL in 5 mL volumetric flasks on a shaker table at room temperature for 10 days. The solutions were cast onto glass plates, allowed to evaporate at room temperature for 1 week, and dried under vacuum at 50 °C for 6 weeks.

Thermal properties of the blends were investigated with DSC using a Perkin-Elmer DSC 7 calibrated against an Indium standard. Approximately 10–15 mg of vacuum dried materials were weighed into aluminum pans and sealed. In all samples, the scanning protocol was: hold at 25 °C for 3 min, heat from 25 °C to 280 °C at 10 °C/min, hold at 280 °C for 5 min, cool from 280 °C to 25 °C at 10 °C/min, hold at 25 °C for 5 min, heat from 25 °C to 280 °C at 10 °C/min.

Thermal stability of the blends was investigated with TGA using a TA Instruments Q500. Samples of 15–25 mg of vacuum dried ground pellets were loaded in an alumina pan and heated under nitrogen from 30 °C to 600 °C.

Dilute solution viscometry of PA410 and PA610 homopolymers was performed on as received pellets, ground pellets after melt-mixing, and test bars after injection molding. For each sample, at least 4 concentrations ranging from 1.5 to 4.5 mg/mL were prepared in m-cresol and the efflux time was measured in an Ubbelohde capillary viscometer at 30 °C.

SAXS and WAXS were performed under vacuum on rectangular bars using an Anton Paar SAXSess. Cu K-α radiation was generated with a PANalytical PW3830 rotating anode source. Each sample was irradiated for 5 min. Reusable image plates were

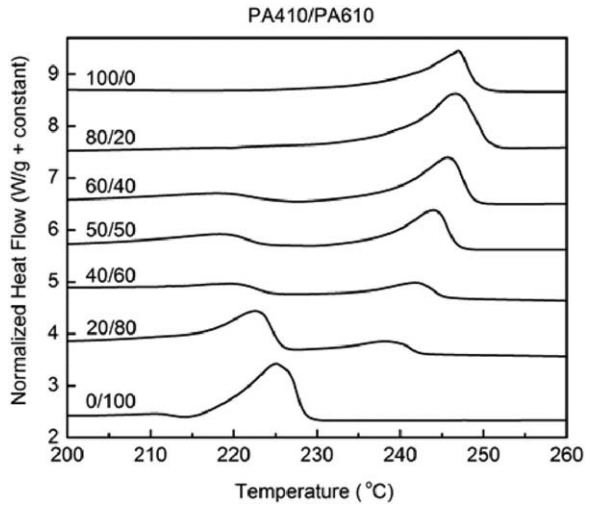

Figure 1. DSC baseline subtracted melting endotherms on second heating of PA410/PA610 wt % melt-mixed blends demonstrating melting point depression of both homopolymers.

analyzed using SAXSQuant-1D software. Intensities were background subtracted and normalized to a Lupolen reference.

DMTA was performed using a Rheometrics ARES-LS rheometer equipped with torsional rectangular fixtures. Rectangular bars were mounted at a clamp force of 40 cN·m. Shear strain of 0.05% was applied at 1 Hz from 25 °C to 180 °C at 10 °C/min. The rheometer was calibrated for normal force and torque prior to each testing session.

Tensile testing was performed according to ASTM D638 using dog bone bars. A minimum of 3 samples for each composition were tested using an Instron 1000 lb_f load cell, a 1-inch Shepic extensometer, and a crosshead speed of 0.1 inch/min.

Notched Izod impact testing was performed using a Testing Machines Inc. pendulum arm impact tester according to ASTM D256. Rectangular bars were notched by hand with a RJW LTD Charpy notch machine with a type H "V" broach. A minimum of three samples for each composition were mounted at a constant clamp force and impacted with a 10 ft-lb_f swing arm.

RESULTS AND DISCUSSION

The PA410/PA610 binary blend system is miscible over all compositions. Melting point depression in a binary polymer blend implies a negative Flory–Huggins interaction parameter thus giving a negative free-energy of mixing.[63,72,77,78] The melting endotherms of melt-mixed PA410/PA610 blends are shown in Figure 1. PA410 melts around 250 °C and PA610 around 230 °C. The melting temperature is defined as the temperature at which the last crystal melts, and was consistently determined from the intersection between one line drawn tangent to the inflection point to the right of the peak and another drawn along the flat section after all traces of crystals have disappeared (an example is shown in the Supporting Information).

On cooling in DSC, the crystallization exotherm peak is used to determine the temperature at which the maximum rate of crystallization occurs. Figure 2 shows the crystallization exotherms of each blend on cooling from the melt. The maximum crystallization rate temperatures for PA410 and PA610 homopolymers, taken to be the temperatures at maximum heat flow, occur at 226 °C and 190 °C, respectively. The maximum crystallization rate temperature decreases as the weight fraction of PA610 is increased with the single exception of the 50 wt % sample.

Nishi and Wang have applied the Flory–Huggins theory of the thermodynamics of polymer mixing to a binary system of two high molecular weight semi-crystalline polymers.[72] The polymer-polymer interaction parameter can be calculated from eq. (1).

$$\chi_{12} = \frac{\Delta H_{2u} V_{1u}}{R V_{2u}} \left(\frac{1}{T_m^o} - \frac{1}{T_m}\right) \left(\frac{1}{(1-\varphi_2)^2}\right) \quad (1)$$

Here, ΔH_{2u} is the equilibrium enthalpy of fusion per repeat unit, V_{1u} and V_{2u} are the molar volumes of repeat units, R is the gas constant, T_m^o and T_m are the pure and depressed equilibrium melting temperatures, respectively, and φ_2 is the polymer volume fraction. The polymer component designated by subscript 2 is the one with the higher melting temperature. From eq. (1) it is clear that melting point depression ($T_m < T_m^o$) implies the interaction parameter is negative.

In the melt-mixed blends very large melting point depression of PA410 crystals were observed, as seen in Figure 1, implying unusually large negative interaction parameters. These large aphysical values were likely influenced by low molecular weight species produced by degradation of polymer chains during melt-mixing. It was therefore necessary to prepare PA410/PA610 solution blends so that degradation could be avoided and interaction parameters could be properly evaluated. Values of melting point depression in solution blends were smaller than in melt-mixed blends, leading to interaction parameter values having reasonable values for hydrogen bonding systems.

The interaction parameter between PA610 and PA410 was calculated as a function of blend composition using eq. (1). Independent parameters needed for the calculation were $\Delta H_{2u} = 67.8$ kJ/mol, $V_{1u} = 271.2$ cm3/mol, $V_{2u} = 238.4$ cm3/

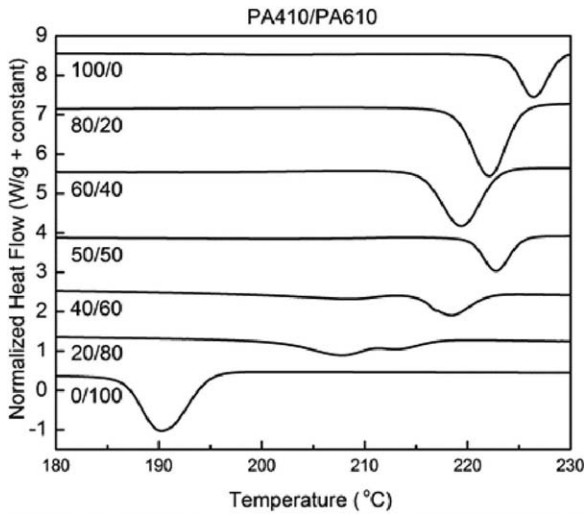

Figure 2. DSC exotherms on cooling from the melt of PA410/PA610 wt % melt-mixed blends.

Table I. Observed Melting Temperatures and Corresponding Interaction Parameters Showing Miscibility over All Compositions

PA410/ PA610 wt %	T_m (°C)	Φ_{PA410}	χ_{12} (kJ/mol)
100/0	250.4 ± 0.3	1	0
80/20	250.1 ± 0.4	0.78	−0.24 ± 0.45
60/40	249.1 ± 0.4	0.59	−0.26 ± 0.13
50/50	248.6 ± 0.9	0.51	−0.25 ± 0.17
40/60	246.7 ± 0.7	0.44	−0.40 ± 0.10
20/80	245.8 ± 0.6	0.21	−0.25 ± 0.05

Table II. Intrinsic Viscosities of PA410 and PA610 Homopolymers before and after Processing

Sample	Intrinsic viscosity (mL/g)
PA410 as received	143 ± 4
PA410 melt blended	101 ± 1
PA410 injection molded	98 ± 1
PA610 as received	129 ± 4
PA610 melt blended	133.2 ± 0.4
PA610 injection molded	131.3 ± 0.5

mol. The results are shown in Table I. All blends exhibit negative interaction parameters, indicating miscibility.

Equation (1) implies the use of equilibrium melting temperatures, or melting temperatures of infinitely thick crystals, but any measured sample has some finite crystal thickness. To accurately compare interaction parameters, one must either assume the same crystal thickness throughout different samples or estimate the equilibrium melting temperature in each sample. For the interaction parameter values reported in Table I, the constant crystal thickness assumption is adopted. With the exception of the 40 wt % PA410 blend, the interaction parameter is found to be roughly independent of composition. Accordingly, the larger melting point depression in the 40 wt % PA410 could be due to a smaller average crystal thickness of that sample.

The extent of degradation throughout the melt mixing and molding processes is an important consideration that influences both thermal and mechanical properties. Thermal stability of the blends was investigated by TGA. The degradation profiles of post-processed blends are shown in Figure 3. All blends exhibit a single-step degradation profile. The degradation temperature (T_{deg}) was calculated as the intersection between lines drawn tangent to the profile before degradation and near the maximum degradation rate, as shown for PA410 in Figure 3. The T_{deg} of all blends was between 438 °C and 439 °C. Less than 1% of the initial mass of any blend degrades until reaching a temperature of 344 °C, well above the processing temperature of 260 °C.

This implies that the temperatures experienced during processing should not cause extensive degradation. However, even with the incorporation of heat stabilizers, slight discoloration of all blends was observed on removal from the mixing bowl. To truly understand the extent of degradation after each processing step, intrinsic viscosities were measured using DSV. The results given in Table II show that PA410 homopolymer degraded much more than PA610 homopolymer during melt blending. Also, the longer mixing duration of 10 min in the melt compared to the shorter duration experienced during injection molding is well reflected by the relative decrease in intrinsic viscosity after each process.

WAXS was used to investigate the types and amounts of crystals formed in the blends. Annealed injection molded bars are used for WAXS studies. The data, shown in Figure 4, exhibit the typical reflections from triclinic α-phases of polyamide crystals. No new reflections are observed, so the possibility of co-crystallization is eliminated. The peak locations were found using a centroid fit and their corresponding d-spacing values are compared with literature values in Table III. The observed d-spacing of PA410 and PA610 homopolymers are in good agreement with previously reported values. Observed diffraction

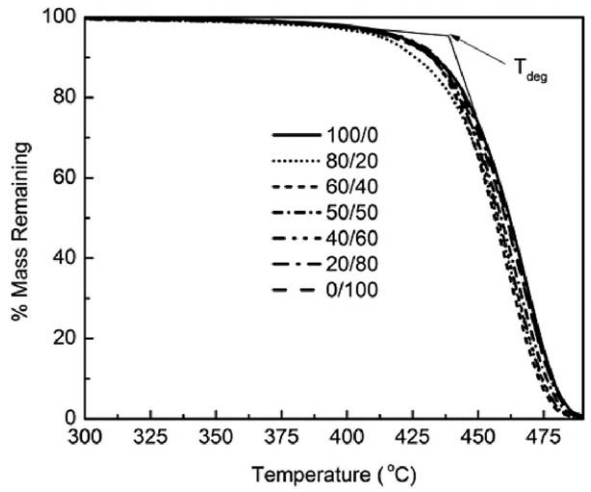

Figure 3. TGA showing degradation of PA410/PA610 wt % blends at temperatures well above processing conditions.

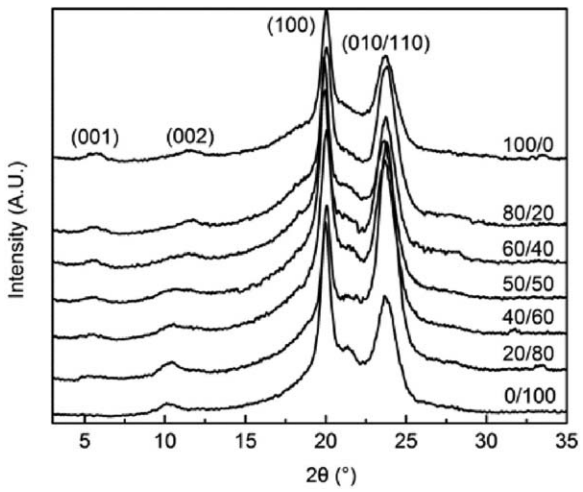

Figure 4. WAXS of PA410/PA610 wt % blends with peaks attributed to reflections from planes represented by Miller Indices.

Table III. Observed d-Spacing and Literature Reported d-Spacing for PA410[79,80] and PA610[80,81]

Miller Indices	001	002	100	010/110
Reported d-spacing (nm)				
PA410	1.561, 1.48	0.776, 0.739	0.442, 0.437	0.379, 0.365
PA610	1.67, 1.68	0.862, 0.842	0.439, 0.441	0.365, 0.374
Observed d-spacing (nm)				
100/0	1.557	0.766	0.443	0.375
80/20	1.605	0.762	0.443	0.374
60/40	1.620	0.772	0.445	0.374
50/50	1.620	0.850	0.445	0.377
40/60	1.605	0.842	0.443	0.376
20/80	1.666	0.858	0.443	0.374
0/100	—	0.862	0.444	0.374

peaks of blends are broader and their corresponding d-spacing values are intermediate values between the homopolymers. This suggests that the two different types of crystals contribute to an average reflection observed in blends.

These data indicate the phenomena of crystallization induced phase separation from a miscible melt state. The two polymers do not co-crystallize as indicated by the absence of new WAXS peaks and the presence of only two distinct melting points in each blend. Locally high concentration regions must be reached before a homopolymer can crystallize; to achieve this high concentration homopolymer must be drawn from the miscible amorphous melt. In the presence of PA410, the PA610 does not crystallize in DSC because it is kinetically restricted over the time scale of the experiment. The cooling rate, however, is not too fast for PA610 to crystallize in the absence of PA410. In high molecular weight polymers, the rate of crystallization is fast compared to the rate of diffusion. Therefore, the crystallization of PA610 is limited by morphological confinement induced by the crystallization of PA410. Conversely, the presence of PA610 does not prevent the crystallization of PA410 in DSC. If the two polymers were phase separated in the melt, they would both be able to crystallize as homopolymers.

The blends were investigated using SAXS as a means of elucidating their morphology. SAXS profiles of annealed injection molded bars are shown in Figure 5. The data exhibit well-defined shoulders corresponding to lamellar long spacings of around 10nm. The lamellar spacing increases and the shoulder becomes narrower with increasing PA610 content. This can be interpreted as there being more PA610 in the amorphous (single phase) interlamellar region leading to an increased long-spacing.

WAXS can also be used to quantify the degree of crystallinity by the deconvolution of amorphous, crystalline, and diffuse scattering intensities.[82] The volume fraction crystallinity of each fully annealed blend composition is calculated according to eq. (2).

$$x_{c,v} = \frac{A_t - A_a}{A_t - A_d} \tag{2}$$

wherein eq. (2) A_t, A_a, and A_d are the areas under the scattering profiles shown in Figure 3 that can be attributed to the total scattering, amorphous scattering, and diffuse scattering, respectively. Details of the deconvolution of scattering intensities for each blend are provided in the Supporting Information.

The volume fraction crystallinity is converted to mass fraction crystallinity using the relationship of eq. (3)

$$x_{c,m} = x_{c,v}\rho_c/\rho \tag{3}$$

where ρ_c, the crystalline density, is calculated using the triclinic α-phase unit cell parameters reported for PA410 and PA610.[80] Values used for ρ_c are 1.224 g/cm^3 for PA410 and 1.198 g/cm^3 for PA610. The overall density, ρ, is estimated by relating the measured transmission of a sample to its expected transmission based on its thickness and its absorption coefficient. Details of the overall density estimations are shown in the Supporting Information.

The mass fraction crystallinity is commonly calculated from DSC measurements through eq. (4).

$$x_{c,m} = \frac{\Delta H_f}{\Delta H_{f,\mathrm{eq}}} \tag{4}$$

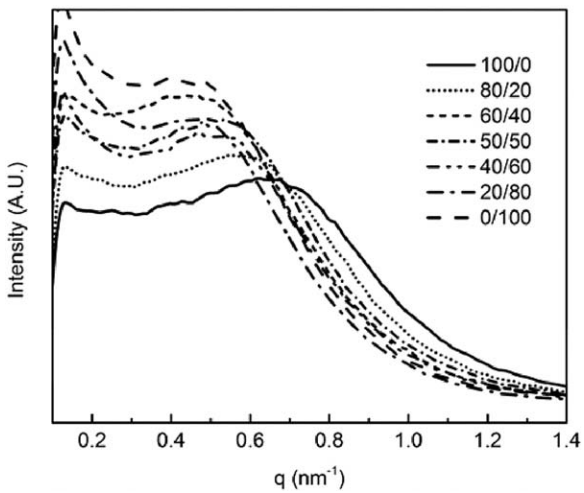

Figure 5. SAXS of PA410/PA610 wt % blends. Intensities are normalized using blank scan, sample thicknesses, and absorption coefficients.

Table IV. Effect of Thermal Annealing on the Degree of Crystallization in Injection Molded Bars of PA410/PA610 Blends

	Unannealed	Annealed	Annealed
PA410/ PA610 wt %	$x_{c,m}$ (DSC)	$x_{c,m}$ (DSC)	$x_{c,m}$ (WAXS)
100/0	0.24	0.35	0.35
80/20	0.21	0.36	0.33
60/40	0.21	0.27	0.29
50/50	0.23	0.32	0.36
40/60	0.23	0.37	0.37
20/80	0.33	0.33	0.40
0/100	0.28	0.39	0.28

DSC measurements taken from first heating scan.

In eq. (4), the equilibrium enthalpy of fusion, $\Delta H_{f,\,eq}$ (the enthalpy required to melt a fully crystalline sample), is an important quantity that must be known to determine crystallinity from DSC measurements. *To the authors' knowledge, the equilibrium enthalpy of fusion has not yet been reported for PA410.* This value can be calculated by rearranging eq. (4) and using the mass fraction crystallinity obtained from WAXS in conjunction with the enthalpy of fusion measured in DSC from the first heating scan of the same fully annealed sample. The equilibrium enthalpy of fusion for PA410 is thus determined to be 269 J/g.

Using a study by Jasinska-Walc *et al.*, the equilibrium enthalpy of fusion for PA410 can be calculated in the same manner, although the authors did not explicitly do so.[79] In the study, WAXS was used to calculate the crystallinity of PA410 during heating and cooling. The melting enthalpy was calculated from DSC using the same heating and cooling conditions. The crystallinity was found to decrease during heating below the melting temperature, but seemed to approach a value of 0.23 in the second heating cycle. The melting enthalpy from the second heating cycle was reported as 67.3 J/g. Using these values, the equilibrium enthalpy of fusion for PA410 can be determined to be 293 J/g, which is similar to the current explicit finding.

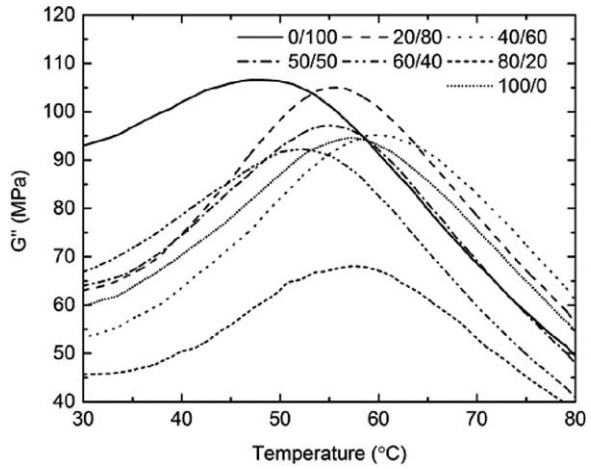

Figure 6. Loss moduli (G″) of PA410/PA610 wt % blends. The peak in G″ occurs over the glass transition temperature region.

Although their structures are similar, PA410 has a higher equilibrium enthalpy of fusion than PA610. This makes sense because PA410 contains a higher number of amide groups (i.e., possible hydrogen bonding sites) per unit mass than PA610. With 2 amide groups for every 14 backbone carbons, PA410 forms a more stable crystal structure leading to a higher melting point. This is also evidenced by the higher crystalline density of PA410 compared to PA610, even though they share the same triclinic crystal form. Knowing the equilibrium enthalpy of fusion enables calculation of the crystalline mass fraction of each sample from DSC measurements using eq. (4). The mass fraction crystallinities calculated by DSC are compared to those calculated by WAXS in Table IV. The mass fraction crystallinities calculated by DSC are in good agreement with those calculated by WAXS showing that the method used to separate the different scattering intensities in WAXS is valid. As expected, thermal annealing increases the degree of crystallization in all blend compositions.

Torsional mechanical properties of annealed blends were investigated over a broad temperature range with DMTA. The loss moduli, G″, of the blends are shown in Figure 6. A peak in the loss moduli indicates α-relaxation, which is the glass transition temperature. All blends appear to exhibit a single peak in G″, which would suggest the presence of only one miscible amorphous phase, but the peaks of the homopolymers are close enough together so that amorphous phase miscibility or immiscibility cannot be concluded. It is interesting to note that the transition, as measured by the width of the G″ peak, is not too much broader in the blends. This indicates a similar amorphous phase molecular environment in the blends and homopolymers. The storage modulus and α-relaxation temperature of each blend is reported in Table V. Homopolymers and blends containing 20 wt % to 40 wt % PA410 all have about the same storage moduli, but 50 wt % to 80 wt % PA410 blends have lower storage moduli. The highest storage modulus is observed in the 20 wt % PA410 blend, which is also the blend that exhibited the highest degree of crystallization.

Tensile testing was performed on blends before and after annealing. The tensile moduli are shown in Figure 7 and the tensile strengths at break in Figure 8. Annealed blends showed

Table V. Storage Modulus (G′) at 30 °C and 1 Hz and α-Relaxation Temperature, Calculated from Peak in G″, of PA410/PA610 wt % Blends

Composition	Storage modulus (GPa)	α-relaxation temperature (°C)
100/0	1.97 ± 0.05	58 ± 3
80/20	1.3 ± 0.3	56 ± 2
60/40	1.73 ± 0.02	52.1 ± 0.8
50/50	1.81 ± 0.04	54.7 ± 0.9
40/60	2.0 ± 0.2	55.2 ± 0.2
20/80	2.09 ± 0.08	55.8 ± 0.8
0/100	1.9 ± 0.1	48 ± 3

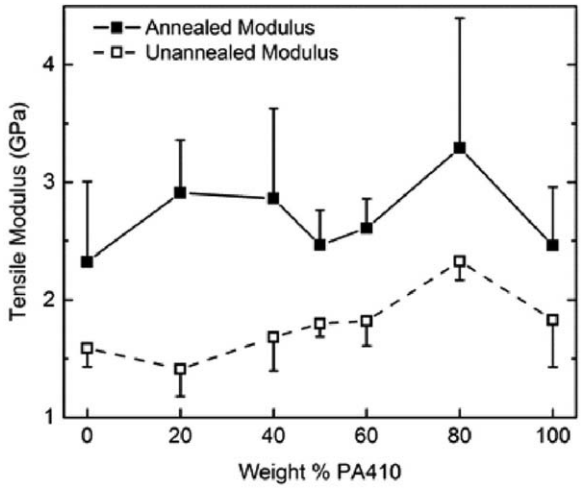

Figure 7. Tensile moduli of PA410 and PA610 blends.

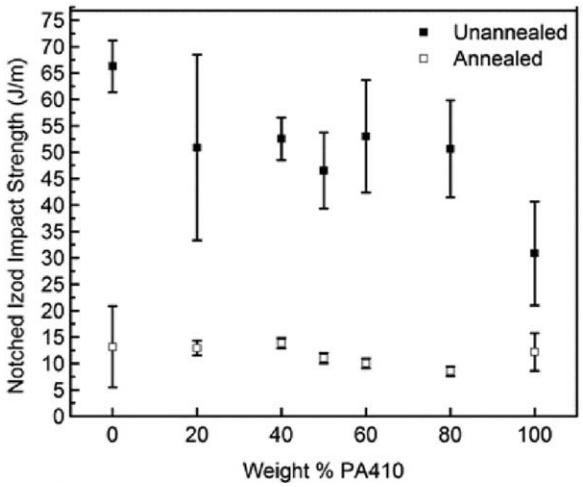

Figure 9. Impact strength of PA410 blended with PA610.

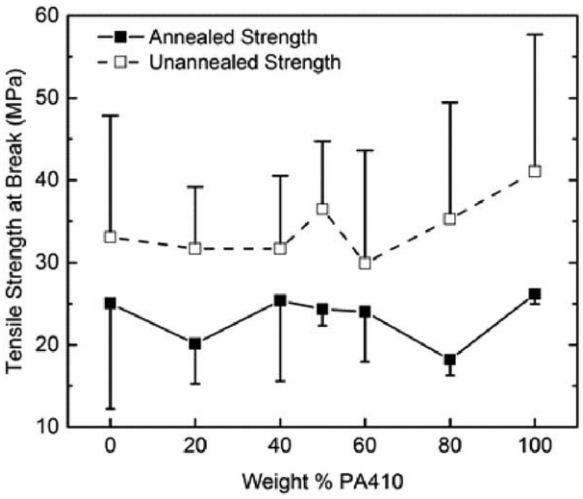

Figure 8. Tensile strength at break of PA410 and PA610 blends.

stress-strain behavior typical of glassy polymers, absent of plastic deformation. Unannealed blends showed behavior more typically associated with nylons, with a yield stress point followed by plastic deformation. As expected, annealing increases the tensile modulus and decreases the tensile strength at break. Chains in amorphous regions are freer to move, allowing straining to greater lengths before fracturing. Crystalline regions provide stiffness but cannot strain to great lengths before fracturing.

Values of annealed tensile moduli seem small compared to values of annealed storage moduli. For polymers with Poisson's ratios of 0.25–0.5, the tensile moduli should be 2.5–3 times larger than the shear moduli given the same crystallinity and moisture content. The current findings for annealed samples show the tensile moduli as 1.5 times larger at most. By comparing unannealed tensile moduli to those specified for PA410 and PA610 in Table VI, the samples used for tensile testing in this study can be associated with a "conditioned" state; that is, they have come to equilibrium with atmospheric moisture. In contrast, the samples used for torsional testing are "dry" (they were tested soon after removal from the annealing oven). Manufacturer specification sheets indicate conditioned moduli are about half as large as dry samples for the homopolymers. Extending this rule to the blends means the tensile moduli are about 3 times larger than the torsional moduli. Therefore, the discrepancy between tensile and torsional moduli is explained by differences in moisture content.

The effect of annealing on impact strength is shown in Figure 9. As expected, the impact strength is much lower in the more crystalline annealed blends. That is, annealing leads to a greater rigid volume fraction which increases modulus but decreases ductility.

Table VI. Physical Properties of Common Polyamides as Specified by Suppliers

Polymer	Grade	Bio-based	Melting point (°C)	Tensile modulus dry/cond (GPa)	Maximum water absorption (%)
PA-6	Ultramid B3K	No	220	3.0/1.0	9-10
PA-6,6	Ultramid A3K	No	260	3.1/1.1	8-9
PA-4,10	EcoPaXX Q150-D	Yes	250	3.1/1.7	5.8
PA-6,10	Ultramid S3K	Yes	220	2.4/1.3	3.6
PA-10,10	Zytel RS LC1000 BK385	Yes	203	2.1/1.2	1.8
PA-11	Rilsan BMNO TLD	Yes	189	NA/1.32	1.9
PA-12	Rilsamid AMVO TLD	No	178	1.4/1.26	1.6

In annealed bars, a positive deviation from a simple mixing law is observed in blends with less than 50 wt % PA410 and negative deviation in blends of 50 wt % and greater PA410. In unannealed bars, the opposite trend is observed.

The tunable thermal properties, through melting point depression, and mechanical properties, which more or less follow a simple mixing law, can be used to meet the design requirements of many engineering applications. Some common physical properties of as molded polyamides with similar uses are compared with PA410 and PA610 in Table VI.

PA410 and PA610 offer superior thermal stability and mechanical rigidity compared to other bio-based polyamides, and less water absorption than other petroleum based polyamides. Flame retardants can be added for safety or chopped fibers for reinforcement when demanding applications require even greater physical properties. Areas of use for PA410 and PA610 include lightweight automotive parts such as engine or crankshaft covers, housings and gear components as well as sporting goods and films for construction or protective coverings.

CONCLUSIONS

Blends of biorenewable PA410 and PA610 are formed by melt mixing. Thermal, mechanical, and morphological properties are investigated using a variety of analytical tools. This combination allows measurement of the equilibrium enthalpy of fusion for PA410 for the first time which is determined to be 269 J/g. Based on melting point depression, negative values of the interaction parameter as a function of composition of about −0.25 (kJ/mol) are found indicating that the blends are miscible over all compositions. Further evidence of miscibility is provided by inhibition of PA610 crystallization during cooling in DSC. Interestingly, the blends exhibit crystallization induced phase separation; both PA410 and PA610 crystals are able to grow on cooling from a miscible melt. WAXS confirms the presence of two distinct crystal types and the absence of co-crystallization.

Mechanical properties are measured on samples before and after annealing. Annealing has significant effects on measured properties. Properties investigated with DMTA, tensile testing, and impact testing are found to follow similar trends with regards to blend composition. Blends containing 20 wt % and 40 wt % PA410 show superior properties, with higher tensile and torsional moduli, impact resistance, and α-relaxation temperatures than either individual homopolymers. This synergistic effect is of important scientific interest.

This binary system exhibits a single amorphous phase but two separate crystalline phases. Miscible systems of two semicrystalline polymers are rare and therefore of basic scientific interest. The results of this study demonstrate that physical properties can be adjusted by varying blend composition. Accordingly, blending of biorenewable polymers is a straightforward strategy to optimize the performance of these emerging materials for a wide variety of applications.

ACKNOWLEDGMENTS

This research was supported under NSF CMMI Grant 1335338 under the SusChem initiative. Support was also provided under a research agreement between the Petroleum Institute of Abu Dhabi and the Colorado School of Mines. The authors would like to thank BASF Chemical Company for their generous donation of PA610 and Chase Plastics for their donation of PA410. WAXS and SAXS measurements were expertly directed by Professor Don L. Williamson of the Colorado School of Mines Physics Department; his support is greatly appreciated.

REFERENCES

1. Plastics News, Study Predicts Sharp Increase in Bioplastics Production by 2018. http://www.plasticsnews.com/article/20141204/NEWS/141209947/study-predicts-sharp-increase-in-bioplastics-production-by-2018 (accessed November 18, **2015**).
2. Plastics News, Study Says Demand for Bioplastics to Grow 19 Percent Annually. http://www.plasticsnews.com/article/20140305/NEWS/140309966/study-says-demand-for-bioplastics-to-grow-19-percent-annually (accessed November 18, **2015**).
3. Ahmann, D.; Dorgan, J. R. *Ind. Biotechnol.* **2007**, *3*, 218.
4. Halley, P. J. D.; John, R. *Mater. Res. Soc. Bull.* **2011**, *36*, 687.
5. Dorgan, J. R. *Macromol. Symp.* **2001**, *175*, 55.
6. Dorgan, J. R.; Janzen, J.; Clayton, M. P.; Knauss, D. M.; Hait, S. B. *J. Rheol.* **2005**, *49*, 607.
7. Braun, B.; Dorgan, J. R.; Knauss, D. M. *J. P. Environ.* **2006**, *14*, 49.
8. Dorgan, J. R.; Janzen, J.; Knauss, D. M.; Hait, S. B.; Limoges, B. R.; Hutchinson, M. H. *J. Polym. Sci. Part B: Polym. Phys.* **2005**, *43*, 3100.
9. Dorgan, J. R.; Lehermeier, H.; Mang, M. *J. Polym. Environ.* **2000**, *8*, 1.
10. Tsuji, H. *Bio-Based Plastics: Mater. Appl.* Kabasci, S., Eds.; Wiley: New Delhi, **2013**, Chapter 8; pp 171–219.
11. Vink, E. T.; Davies, S. *Ind. Biotechnol.* **2015**, *11*, 167.
12. Vink, E. T.; Davies, S.; Kolstad, J. J. *Ind. Biotechnol.* **2010**, *6*, 212.
13. Vink, E. T.; Glassner, D. A.; Kolstad, J. J.; Wooley, R. J.; O'Connor, R. P. *Ind. Biotechnol.* **2007**, *3*, 58.
14. Vink, E. T.; Rábago, K.; Glassner, D. A.; Springs, B.; O'Connor, R. P.; Kolstad, J.; Gruber, P. R. *Macromol. Biosci.* **2004**, *4*, 551.
15. Vink, E. T.; Rabago, K. R.; Glassner, D. A.; Gruber, P. R. *Polym. Degrad. Stab.* **2003**, *80*, 403.
16. Aharoni, S. M. n-Nylons, their Synthesis, Structure, and Properties; Wiley: **1997**.
17. Cicero, J. A.; Dorgan, J. R. *J. Polym. Environ.* **2002**, *9*, 1.
18. Cicero, J. A.; Dorgan, J. R.; Dec, S. F.; Knauss, D. M. *Polym. Degrad. Stab.* **2002**, *78*, 95.
19. Cicero, J. A.; Dorgan, J. R.; Garrett, J.; Runt, J.; Lin, J. S. *J. Appl. Polym. Sci.* **2002**, *86*, 2839.
20. Cicero, J. A.; Dorgan, J. R.; Janzen, J.; Garrett, J.; Runt, J.; Lin, J. S. *J. Appl. Polym Sci.* **2002**, *86*, 2828.
21. Gupta, B.; Revagade, N.; Hilborn, J. *Prog. Polym. Sci.* **2007**, *32*, 455.

22. Okada, A.; Usuki, A. *Macromol. Mater. Eng.* **2006**, *291*, 1449.
23. Braun, B.; Dorgan, J. R.; Hollingsworth, L. O. *Biomacromolecules* **2012**, *13*, 2013.
24. Sobkowicz, M. J.; Braun, B.; Dorgan, J. R. *Green Chem.* **2009**, *11*, 680.
25. Sobkowicz, M. J.; Dorgan, J. R.; Gneshin, K. W. *Aust. J. Chem. (Invited)* **2009**, *62*, 865.
26. Sobkowicz, M. J.; Dorgan, J. R.; Gneshin, K. W.; Herring, A. M.; McKinnon, J. T. *Carbon* **2009**, *47*, 622.
27. Sobkowicz, M. J.; Sosa, R.; Dorgan, J. R. *J. Appl. Polym. Sci.* **2011**, *121*, 2029.
28. Harmsen, P. F. H.; Hackmann, M. M.; Bos, H. L. *Biofuels Bioprod. Biorefin.* **2014**, *8*, 306.
29. Shen, L.; Huafe, J.; Patel, M. K. STS Copernicus Institute for Sustainable Development and Innovation at Utrecht University, Utrecht, Netherlands, **2009**.
30. Dias, E. L.; Shoemaker, J. A. W.; Boussie, T. R.; Murphy, V. J. (Rennovia Inc. USA). U.S. Patent 0,184,495, July 18, **2013**.
31. Fruchey, O. S.; Manzer, L. E.; Dunuwila, D.; Keen, B. T.; Albin, B. A.; Clinton, N. A.; Dombek, B. D. U.S. Patent Application US20140135471 A1: Processes for Producing Butanediol (Bdo), Diaminobutane (Dab), Succinic Dinitrile (Sdn) and Succinamide (Dam) **2011**; p 37.
32. Yu, L.; Dean, K.; Li, L. *Prog. Polym. Sci.* **2006**, *31*, 576.
33. Sionkowska, A. *Prog. Polym. Sci.* **2011**, *36*, 1254.
34. Feldman, D. *J. Macromol. Sci. Pure Appl. Chem.* **2005**, *A42*, 587.
35. Koulouri, E. G.; Scourlis, E. C.; Kallitsis, J. K. *Polymer* **1999**, *40*, 4887.
36. Puglisi, C.; Samperi, F.; Di Giorgi, S.; Montaudo, G. *Macromolecules* **2003**, *36*, 1098.
37. Kuo, S. W. *Polymer* **2008**, *49*, 4420.
38. Paul, D. R.; Barlow, J. W. *Polymer* **1984**, *25*, 487.
39. Nakai, A.; Shiwaku, T.; Wang, W.; Hasegawa, H.; Hashimoto, T. *Macromolecules* **1996**, *29*, 5990.
40. Puskas, J. E.; Kwon, Y.; Altstädt, V.; Kontopoulou, M. *Polymer* **2007**, *48*, 590.
41. Karode, S. K.; Kulkarni, S. S.; Suresh, A. K.; Mashelkar, R. A. *Chem. Eng. Sci.* **1998**, *53*, 2649.
42. Karode, S. K.; Kulkarni, S. S.; Suresh, A. K.; Mashelkar, R. A. *Chem. Eng. Sci.* **1997**, *52*, 3243.
43. Patel, R.; Ruehle, D. A.; Dorgan, J. R.; Halley, P.; Martin, D. *Polym. Eng. Sci.* **2014**, *54*, 1523.
44. Amass, W.; Amass, A.; Tighe, B. *Polym. Int.* **1998**, *47*, 89.
45. Auras, R.; Harte, B.; Selke, S. *Macromol. Biosci.* **2004**, *4*, 835.
46. Chandra, R.; Rustgi, R. *Prog. Polym. Sci.* **1998**, *23*, 1273.
47. Gross, R. A.; Kalra, B. *Science* **2002**, *297*, 803.
48. Ikada, Y.; Tsuji, H. *Macromol. Rapid Commun.* **2000**, *21*, 117.
49. Marra, K. G.; Szem, J. W.; Kumta, P. N.; DiMilla, P. A.; Weiss, L. E. *J. Biomed. Mater. Res.* **1999**, *47*, 324.
50. Martin, O.; Avérous, L. *Polymer* **2001**, *42*, 6209.
51. Samir, M. A. S. A.; Alloin, F.; Dufresne, A. *Biomacromolecules* **2005**, *6*, 612.
52. Sudesh, K.; Abe, H.; Doi, Y. *Prog. Polym. Sci.* **2000**, *25*, 1503.
53. Nair, N. R.; Nampoothiri, K. M.; Pandey, A. *Biotechnol. Lett.* **2012**, *34*, 2031.
54. Nitz, H.; Semke, H.; Mulhaupt, R. *Macromol. Mater. Eng.* **2001**, *286*, 737.
55. Cote, P.; Brisson, J. *Macromolecules* **1994**, *27*, 7329.
56. Ellis, T. S. *Polymer* **1988**, *29*, 2015.
57. Ellis, T. S. *Macromolecules* **1989**, *22*, 742.
58. Ellis, T. S. *Polymer* **1990**, *31*, 1058.
59. Ellis, T. S. *Macromolecules* **1991**, *24*, 3845.
60. Ellis, T. S. *Abstr. Pap. Am. Chem. Soc.* **1992**, *204*, 264.
61. Ellis, T. S. *Macromol. Symp.* **1996**, *112*, 47.
62. Thomas, S. E. *Polymer* **1995**, *36*, 3919.
63. Ruehle, D. A.; Perbix, C.; Castañeda, M.; Dorgan, J. R.; Mittal, V.; Halley, P.; Martin, D. *Polymer* **2013**, *54*, 6961.
64. Zhang, G. Z.; Yoshida, H.; Kawai, T. *Thermochim. Acta* **2004**, *416*, 79.
65. Verma, A.; Deopura, B. L.; Sengupta, A. K. *J. Appl. Polym. Sci.* **1986**, *31*, 747.
66. Wei, M.; Shin, I. D.; Urban, B.; Tonelli, A. E. *J. Polym. Sci. Part B Polym. Phys.* **2004**, *42*, 1369.
67. Adhikari, R.; Michler, G. H. *Prog. Polym. Sci.* **2004**, *29*, 949.
68. Alfonso, G. C.; Russell, T. P. *Macromolecules* **1986**, *19*, 1143.
69. Jo, W. H.; Kwon, I. H. *Macromolecules* **1991**, *24*, 3368.
70. Liu, J. P.; Jungnickel, B. J. *J. Polym. Sci. Part B: Polym. Phys.* **2007**, *45*, 1917.
71. Nedoma, A. J.; Robertson, M. L.; Wanakule, N. S.; Balsara, N. P. *Ind. Eng. Chem. Res.* **2008**, *47*, 3551.
72. Nishi, T.; Wang, T. T. *Macromolecules* **1975**, *8*, 909.
73. Painter, P. C.; Shenoy, S. L.; Bhagwagar, D. E.; Fishburn, J.; Coleman, M. M. *Macromolecules* **1991**, *24*, 5623.
74. Rim, P. B.; Runt, J. P. *Macromolecules* **1983**, *16*, 762.
75. Runt, J.; Gallagher, K. P. *Polym. Commun.* **1991**, *32*, 180.
76. Zhang, H. H.; Prudhomme, R. E. *J. Polym. Sci. Part B Polym. Phys.* **1987**, *25*, 723.
77. Rim, P. B.; Runt, J. P. *Macromolecules* **1984**, *17*, 1520.
78. Scott, R. L. *J. Chem. Phys.* **1949**, *17*, 279.
79. Jasinska-Walc, L.; Villani, M.; Dudenko, D.; van Asselen, O.; Klop, E.; Rastogi, S.; Hansen, M. R.; Koning, C. E. *Macromolecules* **2012**, *45*, 2796.
80. Jones, N.; Atkins, E.; Hill, M.; Cooper, S.; Franco, L. *Polymer* **1997**, *38*, 2689.
81. Dasgupta, S.; Hammond, W. B.; Goddard, W. A. *J. Am. Chem. Soc.* **1996**, *118*, 12291.
82. Alexander, L. E. X-Ray Diffraction Methods in Polymer Science; Wiley: New York, London, Sydney, Toronto, **1969**.